The modulated structure and ferromagnetic insulating state in a nine-layer $BaRuO_3$

2010 J. Phys.: Condens. Matter 22 036003

(http://iopscience.iop.org/0953-8984/22/3/036003)

J. Phys.: Condens. Matter **22** (2010) 036003 (5pp) doi:10.1088/0953-8984/22/3/036003

The modulated structure and ferromagnetic insulating state in a nine-layer $BaRuO_3$

Chao-Hung Du[1], Chang-Hung Yao[1], Dah-Chin Ling[1], Mau-Tsu Tang[2], Fon-Chi Hsu[3], Hsiang-Lin Liu[4], P D Hatton[5] and Naoshi Ikeda[6]

[1] Department of Physics, Tamkang University, Tamsui 25137, Taiwan
[2] National Synchrotron Radiation Research Center, Hsinchu 300, Taiwan
[3] Department of Materials Science, National Tsing Hua University, Hsinchu 300, Taiwan
[4] Department of Physics, National Taiwan Normal University, Taipei, Taiwan
[5] Department of Physics, Durham University, Durham DH1 3LE, UK
[6] Department of Physics, Okayama University, Okayama, Japan

E-mail: chd@mail.tku.edu.tw

Received 11 September 2009, in final form 18 November 2009
Published 21 December 2009
Online at stacks.iop.org/JPhysCM/22/036003

Abstract

We report the observation of a modulated structure and a ferromagnetic insulating state in a high quality single crystal of a nine-layer $BaRuO_3$. Using x-ray scattering, the modulated satellites were observed to double the unit cell along the c-axis at low temperature. The ferromagnetic insulating state is confirmed by magnetic and resistivity measurements. Analyzing the peak profiles from the modulation and host structure respectively, showed a lattice distortion at $T \sim 55$ K. These findings elucidate the intimate relationship between ferromagnetism and lattice distortion in a nine-layer $BaRuO_3$.

(Some figures in this article are in colour only in the electronic version)

1. Introduction

Layered ruthenate compounds have attracted a great deal of attention because of their many unusual physical properties, such as superconductivity in Sr_2RuO_4 [1], and non-Fermi-liquid behavior in $SrRuO_3$ [2, 3]. Because ruthenate oxides possess a rich magnetic phase diagram due to the different coupling strengths between the Ru 4d, O 2p and lattice distortion, they are the model system for studying 4d magnetism [4, 5]. For instance, by partial substitution of Ru with the nonmagnetic element Ti, $CaRuO_3$ displays disorder-induced ferromagnetism [6]. More recently, the family compound $BaRuO_3$ has been observed to exhibit unusual transport behavior on cooling from room temperature; this was ascribed to the formation of a pseudogap [7, 8]. In addition, $BaRuO_3$ undergoes a metal–insulator transition at $T \sim 90$ K, which is thought to be due to the formation of charge-density wave (CDW) modulation. It was reported that, upon further cooling, $BaRuO_3$ displays a weak ferromagnetic transition along the c-axis [7, 9]. The coexistence of charge collective modulation and ferromagnetism was also observed in the family compound $BaIrO_3$ [10, 11].

It is well known that the formation of CDW modulation is accompanied by lattice distortion, which can be observed by x-ray spectroscopy measurements [12]. Furthermore, a distorted lattice has been suggested to play an important role in the ferromagnetic insulating state in hole-doped manganese oxides [13] and $YTiO_3$ [14]. Experimental evidence showing CDW modulation and the interplay between lattice distortion and magnetism in $BaRuO_3$ is lacking. This is probably due to the unknown q vector and the relatively weak diffraction intensities associated with CDW modulation. In this work, a combination of x-ray scattering and image plate and magnetic measurements was performed on a high quality single crystal of a nine-layer $BaRuO_3$. It provides experimental evidence for the presence of a ferromagnetic insulating state, strongly coupled to a complicated lattice distortion associated with CDW modulation, at low temperature.

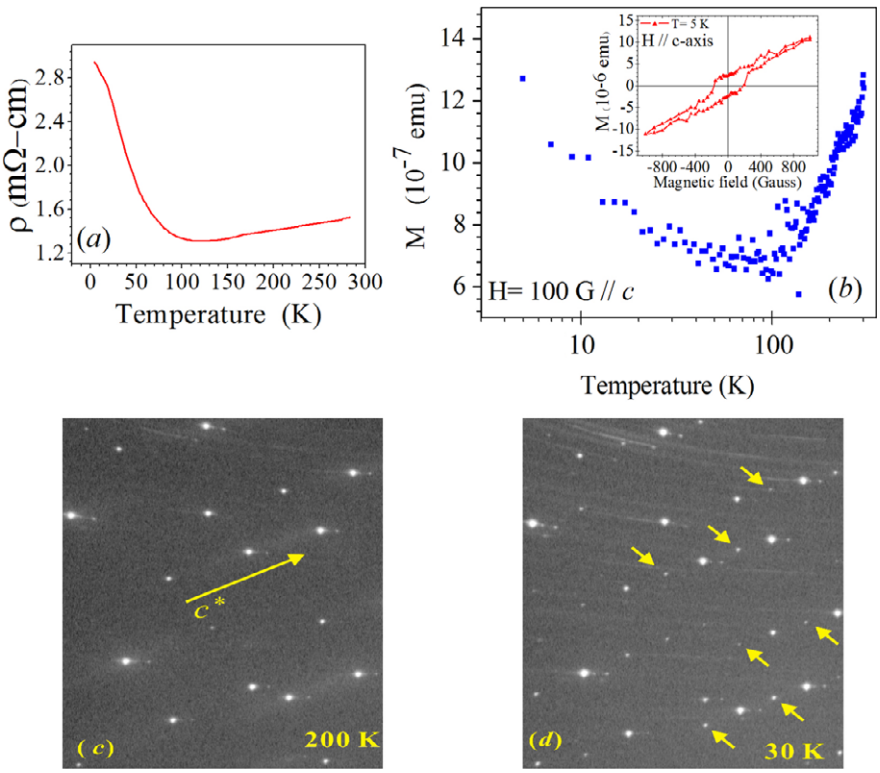

Figure 1. $\rho(T)$, $M(T)$, and diffraction images of $BaRuO_3$. (a) Resistivity measurement shows a metal–insulator transition with a transition temperature of about 90 K. (b) The magnetization measurement with a field of 100 G along the c-axis shows a week ferromagnetic transition at low temperatures. The inset displays the magnetic hysteresis curve at 5 K, confirming the existence of the ferromagnetic state. Diffraction images were taken at (c) $T = 200$ K and (d) at $T = 30$ K, respectively. The yellow arrows indicate the c^*-axis in (c) and some of the satellites in (d).

2. Experiment

A nine-layer $BaRuO_3$ grown by a flux-melting method [15] possesses a hexagonal unit cell with lattice parameters of $a = b = 5.75$ Å and $c = 21.6$ Å [16]. Examined with an in-house x-ray with Cu Kα_1 radiation, this crystal, with a flat surface of about 1×0.7 mm^2, showed a mosaic width of $\sim$0.01° at full width at half maximum (FWHM) for a Bragg peak (0 0 12) and the normal direction along [0 0 1]. For the conductivity measurement, four gold stripes were evaporated on the crystal surface, and a current was applied perpendicular to the [0 0 1] direction. Magnetization measurements were performed using the SQUID magnetometer at National Tsing Hua University. Detailed x-ray measurements were carried out using synchrotron x-rays on beamlines BL02B1 and BL12B2 at SPring-8 in Japan.

3. Results and discussion

3.1. Conductivity and magnetization measurements

A metal–insulator transition observed at $T \sim 90$ K, below which $d\rho/dT$ is less than zero in resistivity measurements, is shown in figure 1(a). This observation is consistent with the reported results for a nine-layer $BaRuO_3$ [7]. This non-linear transport is ascribed to the formation of CDW modulation that distorts the Fermi surface, resulting in a gap opening at the Fermi level [12]. Furthermore, the temperature dependence of magnetization with a field of 100 G along the c-axis also reveals a weak ferromagnetic transition along the c-axis at $T \sim 90$ K, as shown in figure 1(b). These measurements confirm the coexistence of a weak ferromagnetic state and an insulating state in a nine-layered (9R) $BaRuO_3$ at low temperature [7, 9].

As shown in figure 1(b), the magnetization decreases as the temperature decreases from room temperature; it reaches a plateau at $T \sim 90$ K, and increases at $T \sim 55$ K. This decrease was reported by Lee *et al* [7] to be associated with the decrease in carrier density. As the 9R-$BaRuO_3$ possesses a quasi-one-dimensional characteristic along the c-axis, the fluctuations are expected to govern the transport behavior by suppressing the carrier density, resulting in the formation of a pseudogap [17, 18]. This agrees with the transport behavior at high temperature reported by Lee and Rijssenbeek [7, 9]. Noted that the upturn transition at $T \sim 55$ K was only observed by the application of low magnetic fields; it was also observed by Lee and Rijssenbeek. Such a weak ferromagnetic state could result from a local magnetic moment, as observed in $BaIrO_3$ [11]. However, the increase in magnetization below $T \sim 55$ K may also indicate the development of a long-range-ordered ferromagnetic state, which could be stabilized by the lattice distortion [19]. This ferromagnetic state was further confirmed by M–H measurement at 5 K with fields up to 1000 G along the c-axis, as shown in the inset of figure 1(b).

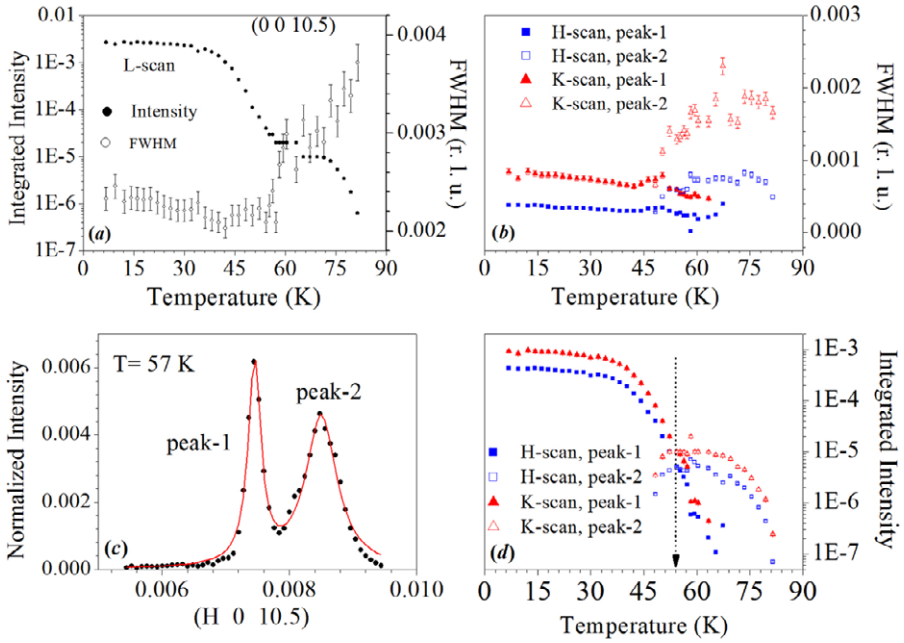

Figure 2. Evolution of the peak profiles of (0 0 10.5) as a function of temperature in the H, K, and L directions. (a) Scans through the L direction. (b) Evolution of the peak widths along the H and K directions. Peak 1 and 2 are marked as shown in (c) and explained in the text. (c) A linear scan through the satellite reflection along the H direction at $T = 57$ K. Both peaks were fitted with the Lorentz function. (d) Changes of the integrated intensity along the H and K directions as a function of temperature. The dotted arrow indicates the transition point, $T \approx 55$ K.

3.2. Synchrotron x-ray measurements

To precisely locate the satellites below the transition temperature, we took diffraction images above and below the transition temperature using an *in-vacuum* camera on beamline BL02B1 at SPring-8. Images taken at $T = 200$ and 30 K are shown in figures 1(c) and (d) for comparison. It is clear that some extra satellites were observed at $T = 30$ K. These satellites were indexed to double the unit cell along the c-axis.

Further studies were carried out by measuring the peak profiles of these satellite reflections, as a function of temperature, on the bending magnet beamline BL12B2. The incident x-rays were selected to be 1 Å by a pair of perfect single crystal Si(1 1 1). High-order contaminations were rejected by a collimating mirror and focusing mirror. The sample used for the image study was glued on a cryostat mounted on a six-circle diffractometer. The multi-circle diffractometer allows the scans to be performed along any crystallographic axis in the reciprocal space. To improve the spatial resolution, a perfect crystal Si(1 1 1) was used as an analyzer. The crystal was aligned with a hexagonal lattice parameter at room temperature and then cooled to 10 K for x-ray scattering measurements. Many satellite reflections were located at positions, such as (0 0 7.5), (0 0 10.5), (0 0 13.5), (0 1 9.5), and (0 1 12.5), suggesting that modulation occurs along the c^* direction and doubles the unit cell along the c-axis. Scans through the three crystallographic axes also show that the modulation possesses anisotropic ordering at low temperature. The ratios of FWHM for ordering along the L, H, and K directions are $W_L/W_H \approx 6$ and $W_K/W_H \approx 2$, respectively, at low temperature, indicating a one-dimensional feature. Figure 2(a) shows scans through the L direction of the satellite reflection (0 0 10.5) as a function of temperature. The integrated intensity decreases with increasing temperature, accompanied by a step-like transition around $T \approx 55$ K and comparatively weak intensities at $T > 80$ K. This agrees with transport data reported for the formation of CDW [7]. After fitting the peak widths with a Lorentz function, the FWHM shows a slight decrease with increasing temperature up to $T \approx 55$ K, above which it exhibits an abrupt increase. This strongly suggests a transition around $T \approx 55$ K.

Figure 2(b) illustrates the evolution of the FWHM as a function of temperature. At low temperature, FWHMs in the H and K directions show a qualitatively similar change to that observed in the L direction. In contrast, as the temperature approaches 48 K from below, the linear scans start to split into two peaks, denoted peak 1 and 2, in the H and K directions, respectively. Peak 1 appears from low temperatures and disappears at about 70 K, while peak 2 appears at about 48 K and persists until about 80 K. Figure 2(c) shows an example of the linear scan through (0 0 10.5) in the H direction at 57 K. Two peaks, which can be fitted with Lorentz functions with different widths, are clearly visible. The changes in the integrated intensity of the satellite reflection also display a step-like transition with a crossover point for peak 1 and 2 at $T \approx 55$ K, as shown in figure 2(d). More remarkably, both peaks 1 and 2 in the H and K directions, respectively, coexist in the temperature range from ∼48 to 68 K.

To understand what was going on in the region of ∼48–68 K, we also performed mesh scans around the satellite (0 0 10.5) as a function of temperature in the real space (i.e. θ–2θ mesh scan), as shown in figure 3. The singlet of the CDW satellite was observed at low temperatures. Upon warming, the

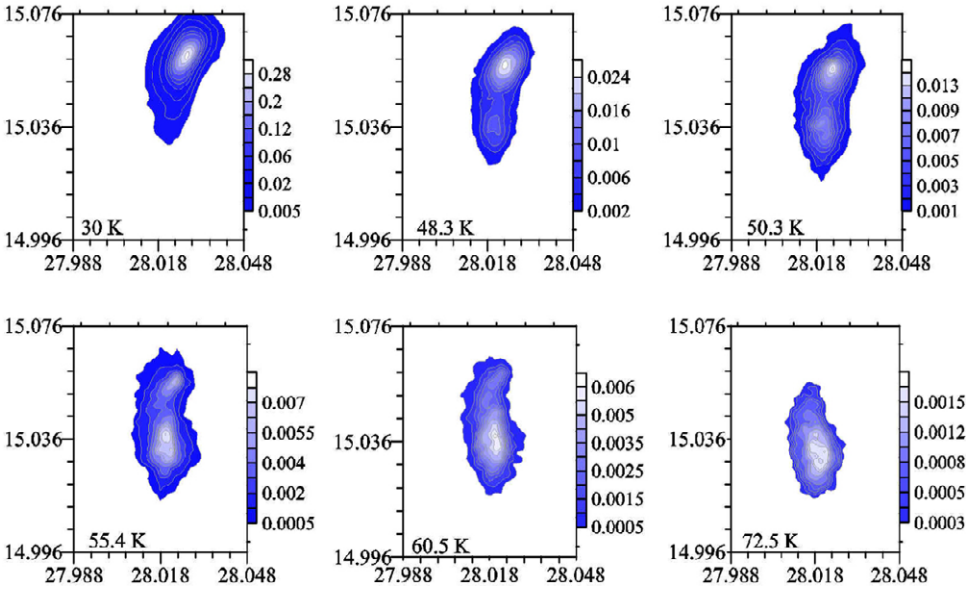

Figure 3. Mesh scans around the CDW satellite (0 0 10.5) at different temperatures. The x-axis presents 2θ and the y-axis presents θ. There is clear splitting of the CDW satellite along the θ-axis at around $T = 55$ K.

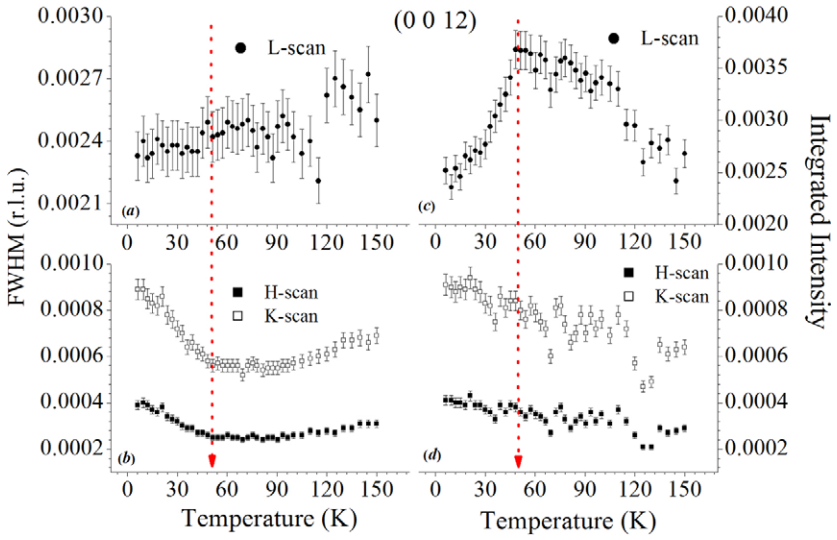

Figure 4. Evolution of the peak profile of (0 0 12) as a function of temperature. (a) Changes of FWHM versus temperature for scans along the L-direction. (b) Changes of FWHM versus temperature for scans along the H- and K-directions. (c) Changes of integrated intensity versus temperature for scans along the L-direction. (d) Changes of integrated intensity versus temperature for scans along the H- and K-directions. Red dotted lines indicate the transition temperature below which an enhancement of magnetization is observed.

satellite started to split at about 48 K along the θ direction. This splitting results in peaks 1 and 2 in the H and K directions, respectively, as shown in figure 2. It becomes a singlet again, with a much weaker signal, at higher temperatures (>68 K). The splitting in the θ direction suggests that it originates from the domain-like structure, and lattice distortion could possibly be responsible for this splitting, as observed in the mesh scans. This splitting only along the θ direction also explains why splitting was not observed in the L-scan. Under this experimental setting, the longitudinal scan in the reciprocal space, along the L direction, corresponds to the θ–2θ scan in real space.

An attempt to further understand the lattice distortion at $T \approx 55$ K was made with linear scans along three crystallographic axes (the H, K, and L directions) through reflections from the host lattice, such as (0 0 9), (0 0 12), and (0 0 15). Figure 4 illustrates the representative results from the Bragg reflection (0 0 12). Upon cooling through the transition temperature, $T \approx 80$ K, for the formation of CDW, the peak profile does not show the character of phase transition, suggesting that the appearance of modulation at $T \approx 80$ K is not caused by a structural phase transition. This is consistent with the formation of CDW [12]. As shown in figure 4(a), in the scans through the L direction of the

Bragg peak (0 0 12), the FWHM of the peak profile does not show any substantial change at low temperature. The corresponding integrated intensity, however, starts to drop at $T \approx 55$ K, as shown in figure 4(c). In contrast to scans in the L direction, FWHMs in the H and K directions increase below $T \approx 55$ K, and the integrated intensities in the H and K directions increase slightly at low temperature, as shown in figures 4(b) and (d), respectively. The increase in the peak profiles suggests that the ordering of the host lattice, on the $a^* \times b^*$ plane, becomes shorter. This anisotropic change is in accord with that observed by Lee using Raman spectra [17]. In their study, the phonon vibration modes A_{1g} and E_g showed opposite vibration behavior, which results in an anisotropic change along the c^* and $a^* \times b^*$. This anisotropic change could be also associated with an in-plane rotation of the RuO_6 octahedron. Such a transition occurring at $T \approx 55$ K is also in accord with the weak ferromagnetic transition, as shown in figure 1(b). It was argued that contamination by a small amount of magnetic impurities during crystal growth could cause the upturn in magnetic susceptibility at 55 K [7]. However, it is unlikely in this case, because the contamination of impurities cannot be responsible for the peak broadening and the decrease of integrated intensity from the CDW and Bragg reflections at low temperature.

4. Conclusions

In conclusion, we demonstrated the interplay between ferromagnetism and lattice distortion in a nine-layer $BaRuO_3$ using x-ray scattering and magnetic measurements. Above the transition temperature T_{CDW} (∼80 K) for the formation of CDW, charge fluctuations arising from the quasi-one-dimensional characteristic along the c-axis could possibly induce a temperature-dependent pseudogap. This reduces the density of states at the Fermi level and manifests itself as a decrease in magnetic susceptibility. As the temperature approaches T_{CDW}, the development of CDW turns the pseudogap into a true gap-like character and results in the metal–insulator transition. Accordingly, the lattice distortion induced by the CDW somehow stabilizes the alignment of electron spins, giving rise to a plateau in $M(T)$ at $T \sim T_{CDW}$. Below T_{CDW}, the lattice distortion, as observed from the changes in the peak profiles of Bragg reflections from the host lattice, significantly enhances the magnetization at low temperature. However, we still cannot identify the origin of the lattice distortion[7], and more detailed crystallographic and local magnetization studies, such as the use of high resolution x-ray diffraction and muon-spin relaxation techniques at low temperature, are required.

Acknowledgments

CHD and DCL are indebted to the National Science Council and Tamkang University for financial support, through the grant Nos NSC 96-2112-M-032-009-MY3, 97-2120-M-007-012, and 96-2212-M-032-008-MY3. CHD is also grateful to Professor Cheng Chung Chi for fruitful discussions. The beam time arrangements by the NSRRC and SPring-8 are also gratefully acknowledged.

References

[1] Maeno Y, Hashimoto H, Yoshida K, Nishizaki S, Fujita T, Bednorz J G and Lichtenberg F 1994 *Nature* **372** 532
[2] Kostic P, Okada Y, Collins N C, Schlesinger Z, Reiner J W, Klein L, Kapitulnik A, Geballe T H and Beasley M R 1998 *Phys. Rev. Lett.* **81** 2498
[3] Puchkov A V, Schabel M C, Basov D N, Startseva T, Gao G, Timusk T and Shen Z-X 1998 *Phys. Rev. Lett.* **81** 2747
[4] Mazin I and Singh D J 1997 *Phys. Rev.* B **56** 2556
[5] Vidya R, Ravindran P, Kjekshus A, Fjellvåg H and Hauback B C 2004 *J. Solid State Chem.* **177** 146
[6] He T and Cava R J 2001 *Phys. Rev.* B **63** 172403
[7] Lee Y S, Lee J S, Kim K W, Noh T W, Yu J, Bang Y, Lee M K and Eom C B 2001 *Phys. Rev.* B **64** 165109
[8] Lee Y S, Lee J S, Kim K W, Noh T W, Yu J, Choi E J, Cao G and Crow J E 2001 *Europhys. Lett.* **55** 280
[9] Rijssenbeek J T, Jin R, Zadorozhny Y, Liu Y, Batlogg B and Cava R J 1999 *Phys. Rev.* B **59** 4561
[10] Cao G, Crow J E, Guertin R P, Henning P F, Homes C C, Strongin M, Basov D N and Lochner E 2000 *Solid State Commun.* **113** 657
[11] Brooks M L, Blundell S J, Lancaster T, Hayes W, Pratt F L, Frampton P P and Battle P D 2005 *Phys. Rev.* B **71** 220411
[12] Grüner G 1994 *Density Waves in Solids* (New York: Addison-Wesley)
[13] Urushibra A, Moritomo Y, Arima T, Asamitsu A, Kido G and Tokura Y 1995 *Phys. Rev.* B **51** 14103
[14] Ulrich C, Khaliullin G, Okamoto S, Reehuis M, Ivanov A, He H, Taguchi Y, Tokura Y and Keimer B 2002 *Phys. Rev. Lett.* **89** 167202
[15] Shepard M, McCall S, Gao G and Crow J E 1997 *J. Appl. Phys.* **81** 4978
[16] Donohue P C, Katz L and Ward R 1965 *Inorg. Chem.* **4** 306
[17] Lee Y S, Noh T W, Park J H, Lee K B, Gao G, Crow J E, Lee M K, Eom C B, Oh E J and Yang I-S 2002 *Phys. Rev.* B **65** 235113
[18] Posazhennikova A and Coleman P 2003 *Phys. Rev.* B **67** 165109
[19] Matzdorf R, Fang Z, Ismail, Zhang J, Kimura T, Tokura Y, Terakura K and Plummer E W 2000 *Science* **289** 746

[7] According to the published reports, we assigned the satellite reflections, as reported in this study, to be caused by the formation of CDWs.